Distinct temporal filters in mitral cells and external tufted cells of the olfactory bulb

Christopher E Vaaga[1,2], Gary L Westbrook[1]

[1] Vollum Institute, Oregon Health and Science University, Portland OR, USA

[2] Neuroscience Graduate Program, Oregon Health and Science University, Portland OR, USA

Corresponding Author:

Christopher E Vaaga

L474, Vollum Institute

3181 SW Sam Jackson Park Rd

Portland OR, 97239

vaaga@ohsu.edu

Running Title: Temporal filters in the olfactory bulb

Acknowledgements: We thank Dr. Henrique von Gersdorff and members of the Westbrook lab for helpful comments on this manuscript. This work was supported by a NS26494 (GLW, a National Science Foundation Graduate Research Fellowship DGE 0925180 (CEV), and a LaCroute Neurobiology of Disease fellowship (CEV).

Abstract: 249
Key Points: 148
Introduction: 343
Discussion: 1346
Pages: 28
Figures: 5

Abstract:

Short-term synaptic plasticity is a critical regulator of neural circuits, and largely determines how information is temporally processed. In the olfactory bulb, afferent olfactory receptor neurons respond to increasing concentrations of odorants with barrages of action potentials, and their terminals have an extraordinarily high release probability (Sicard, 1986; Murphy *et al.,* 2004). These features suggest that during naturalistic stimuli, afferent input to the olfactory bulb is subject to strong synaptic depression, presumably truncating the postsynaptic response to afferent stimuli. To examine this issue, we used single glomerular stimulation in mouse olfactory bulb slices to measure the synaptic dynamics of afferent-evoked input at physiological stimulus frequencies. In cell-attached recordings, mitral cells responded to high frequency stimulation with sustained responses, whereas external tufted cells responded transiently. Consistent with previous reports (Murphy *et al.*, 2004), olfactory nerve terminals onto both cell types had a high release probability (0.7), from a single pool of slowly recycling vesicles, indicating that the distinct responses of mitral and external tufted cells to high frequency stimulation did not originate presyaptically. Rather, distinct temporal response profiles in mitral cells and external tufted cells could be attributed to slow dendrodendritic responses in mitral cells, as blocking this slow current in mitral cells converted mitral cell responses to a transient response profile, typical of external tufted cells. Our results suggest that despite strong axodendritic synaptic depression, the balance of axodendritic and dendrodendritic circuitry in external tufted cells and mitral cells, respectively, tunes the postsynaptic responses to high frequency, naturalistic stimulation.

Key Points:

- The release probability of the ORN is reportedly one of the highest in the brain (Murphy et al., 2004), which is predicted to impose a transient temporal filter on postsynaptic cells.
- Mitral cells responded to high frequency ORN stimulation with sustained transmission, whereas external tufted cells responded transiently.
- The release probability of ORNs (0.7) was equivalent across mitral and external tufted cells and could be explained by a single pool of slowly recycling vesicles.
- The sustained response in mitral cells resulted from dendrodendritic amplification in mitral cells, which was blocked by NMDA and mGluR1 receptor antagonists, converting mitral cell responses to transient response profiles.
- Our results suggest that although the afferent ORN synapse shows strong synaptic depression, dendrodendritic circuitry in mitral cells produces robust amplification of brief afferent input, thus the relative strength of axodendritic and dendrodendritic input determines the postsynaptic response profile.

Introduction:

The computational capacity of neural circuits is largely determined by the short-term synaptic dynamics within the circuit (Abbott & Regehr, 2004), as determined by pre- and postsynaptic mechanisms. Short-term synaptic depression, which generally occurs at high release probability synapses, results in a net decrease in postsynaptic responses with repeated stimulation, and is often attributed to depletion of the readily releasable pool of synaptic vesicles (Liley & North, 1953; Betz, 1970; von Gersdorff & Borst, 2002; Regehr, 2012). However, at some synapses, multiple pools of synaptic vesicles with distinct release probabilities can protect the circuit from synaptic depression during high frequency stimulation (Lu & Trussell, 2016; Taschenberger *et al.*, 2016; Turecek *et al.*, 2016).

In the olfactory bulb, principal neurons receive monosynaptic input from olfactory receptor neuron afferents (Gire & Schoppa, 2009; Najac *et al.*, 2011; Gire *et al.*, 2012; Vaaga & Westbrook, 2016). Odorant receptor neurons (ORNs) respond to increasing odorant concentrations with monotonic increases in firing frequency up to 100 Hz (Sicard, 1986; Duchamp-Viret *et al.*, 1999; Rospars *et al.*, 2003; Tan *et al.*, 2010). Furthermore, the release probability of the afferent synapse between the ORN and its postsynaptic targets is one of the highest reported in the brain (ca. 0.8-0.9; Murphy *et al.*, 2004). Together, these features suggest that the transmission between ORNs and principal neurons is subject to robust short-term depression. However, *in vivo,* mitral cells respond to olfactory input with sustained responses (Giraudet *et al.*, 2002; Nagayama *et al.*, 2004; Leng *et al.*, 2014), suggesting either that release probability during trains is not as high as has been reported, or other circuit mechanisms maintain sustained transmission.

To examine the synaptic dynamics between ORN afferents and principal neurons in response to physiologically relevant stimulation frequencies, we recorded the postsynaptic

97 responses of mitral cells and external tufted cells during high frequency afferent stimulation. Our
98 results suggest that the high release probability and slow vesicle dynamics within the ORN are
99 optimized for faithful transmission, but dendrodendritic amplification in mitral cells compensates
100 for the strong synaptic depression and strongly amplifies afferent input.
101
102 **Materials and Methods:**
103 *Animals*: We used adult (>p24) male and female C57Bl6/J as well as Tg(Thy1-YFP) GJrs
104 heterozygous mice. The Oregon Health and Science University Institutional Animal Care and
105 Use Committee approved all animal procedures.
106 *Slice Preparation:* Olfactory bulb slices were prepared as described previously (Schoppa
107 & Westbrook, 2001). Mice were given an intraperitoneal injection of 2% 2,2,2-tribromoethanol
108 (0.7-0.8 mL) and monitored until fully anesthetized, then transcardially perfused with
109 oxygenated 4º C modified ACSF solution, which contained (in mM): 83 NaCl, 2.5 KCl, 1
110 NaH_2PO_4, 26.2 $NaHCO_3$, 22 dextrose, 72 sucrose, 0.5 $CaCl_2$, 3.3 $MgSO_4$ (300-310 mOsm, pH:
111 7.3). The brain was quickly removed and coronally blocked at the level of the striatum.
112 Horizontal sections (300 μm) through the olfactory bulb were made using a Leica 1200S
113 vibratome. Slices were recovered in warm (32-36º C) ACSF for 30 minutes then were stored at
114 room temperature until transfer to the recording chamber. Unless otherwise noted, the ACSF
115 contained (in mM): 125 NaCl, 25 $NaHCO_3$, 1.25 NaH_2PO_4, 3 KCl, 2.5 dextrose, 2 $CaCl_2$, 1
116 $MgCl_2$ (300-310 mOsm, pH: 7.3).
117 *Electrophysiology:* Whole cell voltage clamp and current clamp recordings were made
118 from mitral cells and external tufted cells under DIC optics. Mitral cells and external tufted cells
119 were identified as described previously (Hayar *et al.*, 2005; Vaaga & Westbrook, 2016). Briefly,

mitral cells were identified by their soma position within the mitral cell layer and external tufted cells were identified by their relatively large soma position within the outer 2/3 of the glomerular layer. Patch pipettes (3-5 MΩ) contained (in mM): 120 K-gluconate, 20 KCl, 10 HEPES, 0.1 EGTA, 4 Mg-ATP, 0.3 Na-GTP, 0.05 Alexa-594 hydrazide, and 5 QX-314. We made no correction for the liquid junction potential (-7 mV). During cell-attached recordings, the membrane patch was held at -70 mV after achieving a gigaohm seal. Data were acquired using a Multiclamp 700b amplifier (Molecular Devices, Sunnyvale CA, USA) and AxographX acquisition software. Data was digitized at 10 kHz and low pass Bessel filtered at 4 KHz. For cell-attached recordings, the data was filtered post-hoc at 1 kHz. During whole-cell recordings the series resistance was continually monitored with a -10 mV hyperpolarizing step. Series resistance was generally <25 MΩ and was not compensated. Cells with greater than 30% change in series resistance during the recording were excluded from analysis. For better visualization, all recordings were made at 34-36º C.

EPSCs were elicited using single glomerulus theta stimulation, as described previously (Vaaga & Westbrook, 2016). Stimulation was provided by a constant current stimulator (100 µs, 3.2 - 32 mA) in conjunction with a small bore theta electrode (2 µm) placed directly in the axon bundle entering the target glomerulus. All recordings were made along the medial aspect of the olfactory bulb, and recordings were only made if the ORN bundle entering the target glomerulus was clearly identifiable under DIC optics. Stimulation trains (10, 25 and 50 Hz, 20 pulses) were chosen to represent the approximate firing rate of ORNs in response to odorant presentation (Sicard, 1986; Duchamp-Viret *et al.*, 1999; Carey *et al.*, 2009; Tan *et al.*, 2010). ORN stimulation was repeated at 60-second intervals, to prevent rundown. All drugs were prepared from stock solutions according to manufacturer specifications and applied via a gravity fed

perfusion system. The drugs used included: 2 mM kynurenic acid, 500 nM sulpiride, 200 nM CGP55845, 10 µM CPP and 20 µM CPCCOEt. All drugs were purchased from Abcam Biochemical (Cambridge, MA, USA) or Tocris Biosciences (Ellisville, MO, USA).

Data Analysis. Electrophysiology data was analyzed using AxographX (www.axograph.com) and IGOR Pro (version 6.22A, Wavemetrics). Spike waveforms in cell-attached recordings were detected using a threshold detection criteria in AxographX, which was used to calculate the total spike number and to generate raster plots. Voltage clamp traces represent the average of 5-10 sweeps after baseline subtraction. Fast EPSC amplitude measurements were made foot-to-peak, to eliminate any contribution of the slow current. To directly measure the slow current we recorded the EPSC amplitude just prior to each stimulus within the train. The total charge transfer (0 – 2.5 seconds after stimulus onset) was measured using a built-in AxographX routine. Data was normalized to the first fast peak EPSC amplitude, unless otherwise noted.

To estimate release probability, we used two methods to calculate the size of the readily releasable pool, each of which utilizes different assumptions (Neher, 2015; Thanawala & Regehr, 2016). In the Schneggenburger, Meyer and Neher method (SMN method), the cumulative fast EPSC amplitude (at 50 Hz stimulation) was plotted as a function of stimulus number and a linear fit was made using the last 5 responses in the train. The readily releasable pool size was estimated as the y-intercept of the linear fit (Schneggenburger *et al.*, 1999, 2002), and release probability was calculated by dividing the initial EPSC amplitude by the size of the readily releasable pool. In the Elmqvist-Quastal method (EQ method; (Elmqvist & Quastel, 1965), the fast EPSC amplitude was plotted as a function of the cumulative EPSC amplitude. A

linear fit to the first 3 EPSCs was used to calculate the size of the readily releasable pool (x-intercept). Release probability was then calculated as in the SMN method.

Statistics: All data is reported as mean±SEM unless otherwise indicated. Statistical analysis was performed in Prism6 (GraphPad Software, La Jolla, CA). One-way and two-way repeated measure experiments were analyzed using ANOVA with Holm-Sidak post-hoc pairwise comparisons as indicated in the text. To compare the exponential fit across data sets, an extra sum of squares F-test was performed to compare lines of best fit. In agreement with previous electrophysiological studies, the data was assumed to be normally distributed, and was thus analyzed using parametric statistics. Student's paired and unpaired t-tests were used as appropriate. Sample sizes were chosen to detect an effect size of 20%, based on prior, similar experiments, with a power of 0.8. In all experiments, the initial value for α was set to $p<0.05$, and was adjusted for multiple comparisons as appropriate.

Results:

Different temporal response profiles in mitral and external tufted cells

To examine the synaptic dynamics of principal neuron activity in response to high frequency afferent stimulation, we first measured the spiking of mitral and external tufted cells using cell-attached recordings. Both cell types responded to 50 Hz ORN stimulation with spikes throughout the stimulus train (Figure 1 A-D). Mitral cells and external tufted cells produced similar numbers of spikes early in the train, however, action potentials in external tufted cells gradually decreased, such that by the 7th stimulus, mitral cells produced more action potentials per successive stimulus than external tufted cells (two-way ANOVA; $p<0.01$; n=7 mitral cells, 8 external tufted cells; Figure 1 E). Likewise, mitral cells continued to spike well after the end of

188 the stimulus train, contributing to the higher total number of spikes produced (mitral cells:
189 161.8±27.2 spikes per trial, n=7 cells; external tufted cells: 45.2±9.0 spikes per trial, n=8 cells,
190 2.5 second window, unpaired t-test: p=0.009, Figure 1 F).
191 In order to quantify the temporal filter in mitral cells and external tufted cells, we
192 calculated the percentage of the total spikes that occurred within 20 ms of each stimulus within
193 the 50 Hz train. Using this metric, a steep input-output curve is indicative of a transient temporal
194 filter. In both mitral cells and external tufted cells, the input-output curve was fit by a single
195 exponential decay. In mitral cells, this relationship was relatively shallow (τ=5.2 stimuli),
196 consistent with the observed sustained transmission. On average, mitral cells produced 7.8±2.7%
197 of total spikes immediately after the first stimulus and 3.8±1.0% of spikes following the final
198 stimulus (n=7 cells). In contrast, external tufted cells had a much steeper input-output
199 relationship (τ=3.2 stimuli), producing 13.7±4.0% of total spikes after the first stimulus and
200 2.8±0.47% following the final stimulus (extra sum of squares F test: $p<0.0001$, n=8 cells). Thus
201 the two cell types have distinct response properties with mitral cells responding to high
202 frequency stimulation with a sustained response, whereas external tufted cells respond
203 transiently.
204
205 *High release probability from a single pool of synaptic vesicles*
206 Differences in release probability of ORN terminals could underlie the distinct responses
207 of mitral cells and external tufted cells, as release probability was only examined in tufted cells
208 (Murphy *et al*., 2004). To determine the release probability, we stimulated at high frequencies to
209 estimate the size of the readily releasable pool using two analytical approaches as described in
210 the methods (Elmqvist & Quastel, 1965; Schneggenburger *et al.*, 1999; Neher, 2015; Thanawala

& Regehr, 2016). Consistent with a high release probability synapse, 50 Hz trains of stimuli elicited robust depression of the phasic EPSC amplitude in mitral cells (Figure 2 A_1) and external tufted cells (Figure 2 B_1). Both the SMN method (Figure 2 A_2, and B_2, C) and EQ method (Figure 2 A_3, and B_3, C) yielded similar estimates of the size of the readily releasable pool in mitral cells and external tufted cells. Accordingly, there was no difference in the release probability between cell types (SMN: mitral cells: 0.67±0.02, n=7 cells, external tufted cells: 0.71±0.06, n=8 cells, p=0.51; EQ: mitral cells: 0.66±0.02, external tufted cells: 0.73±0.03, p=0.14; Figure 2 C). These results indicate that the release probability of ORNs is high, but somewhat lower than previous estimates in tufted cells (Murphy *et al.*, 2004), which likely reflects the activation of presynaptic D_2 and $GABA_B$ receptors in our experiments (Nickell *et al.*, 1994; Aroniadou-Anderjaska *et al.*, 2000; Ennis *et al.*, 2001; Wachowiak *et al.*, 2005; Maher & Westbrook, 2008; Shao *et al.*, 2009; Vaaga *et al.*, 2017). Consistent with this hypothesis, measurements of the release probability in D_2 and $GABA_B$ receptor antagonists (500 nM sulpiride and 200 nM CGP55845, respectively) increased the release probability to 0.95±0.06 (SMN method, n=4 cells, unpaired t-test: p=0.008). Furthermore, 2 mM kynurenic acid, which blocks receptor saturation and desensitization (Trussell *et al.*, 1993; Wadiche & Jahr, 2001; Foster *et al.*, 2002; Wong *et al.*, 2003; Chanda & Xu-Friedman, 2010) did not affect the paired pulse ratio (control: 0.24±0.05; 2 mM kynurenic acid: 0.25±0.05, n=5 cells, paired t-test: 0.70; Figure 2 D, E), suggesting that at the ORN afferent synapse, synaptic depression is primarily mediated by presynaptic factors, and is consistent with univesicular release (Murphy *et al.*, 2004; Taschenberger *et al., 2016*).

In other circuits (Mennerick & Matthews, 1996; Sakaba & Neher, 2001; Lu & Trussell, 2016; Turecek *et al.*, 2016), multiple pools of synaptic vesicles have heterogeneous release

probabilities, which, if present, could obscure our measurements of release probability and support sustained transmission at high stimulation frequencies (Neher, 2015; Turecek *et al.*, 2016). To test for the presence of multiple pools of synaptic vesicles, we stimulated at 10 Hz (20 pulses) to deplete the high release probability pool then switched to 50 Hz stimulation (20 pulses), a protocol that has been used to reveal a transient facilitation resulting from the low release probability of a separate pool of vesicles (Lu & Trussell, 2016; Turecek *et al.*, 2016). In external tufted cells this stimulation protocol failed to elicit facilitation (Figure 3 A); rather, switching to high frequency stimulation elicited further depression of the ORN-evoked phasic EPSC ($EPSC_{21}$: 25.3±0.4% of control, $EPSC_{22}$: 14.7±0.2% of control; Figure 3 B), suggesting a single pool of synaptic vesicles. Likewise, the decay of the phasic EPSC amplitude of external tufted cells as a function of stimulus number was best fit with a single exponential function (τ: 0.68; extra sum of squares F test: p=0.49; Figure 3 C). Together, these data indicate that a single pool of high release probability vesicles is sufficient to explain release from afferent olfactory nerve terminals.

Sustained responses in some cases can be maintained despite high release probability as a result of fast vesicle replenishment (Wang & Kaczmarek, 1998; Saviane & Silver, 2006). However, the phasic EPSC amplitude recovered surprisingly slowly, following a double exponential time course (τ_1: 0.79 seconds; τ_2: 8.23 seconds, Figure 3 D-F), suggesting that fast vesicle replenishment does not contribute to the sustained responses in mitral cells.

Dendrodendritic excitation maintains sustained transmission

Our results suggest that properties of the afferent presynaptic terminal alone cannot explain the sustained transmission observed in mitral cells. To determine what mechanisms

support sustained transmission we examined the responses of mitral cells and external tufted cells in voltage clamp following stimulation across a range of stimulus frequencies (10 Hz, 25 Hz, 50 Hz; Figure 4 A, B). Across stimulus frequencies, the phasic EPSC showed robust depression (Figure 4 D, E). Surprisingly, even relatively low stimulus frequencies (10 Hz) elicited strong depression in mitral and external tufted cells, consistent with the slow vesicle replenishment rates and unusually high release probability. In both cell types, there was a significant effect of stimulus frequency on the degree of phasic EPSC depression (One way ANOVA: mitral cell: $p=0.0003$; external tufted cell: $p<0.0001$). In both cells, the depression increased from 10 Hz to 25 Hz (mitral cells: 10 Hz: 16.4±1.3% of $EPSC_1$, n=6 cells; 25 Hz: 9.4±2.1% of $EPSC_1$ n=5 cells, Holm-Sidak post-hoc comparison: $p<0.05$; external tufted cells: 10 Hz: 14.8±2.0, n=7 cells; 25 Hz: 5.8±0.9% of control, n=7, Holm-Sidak post-hoc comparison: $p<0.001$), but was not significantly different between 25 Hz and 50 Hz (mitral cell: 25 Hz: 9.4±2.1% of $EPSC_1$ n=5 cells, 50 Hz: 5.4±0.9% of $EPSC_1$, n=6 cells, Holm-Sidak post-hoc comparison: $p>0.05$; external tufted cell: 25 Hz: 5.8±0.9% of $EPSC_1$, n=7, 50 Hz: 4.4±0.6% of $EPSC_1$, n=8 cells, Holm-Sidak post-hoc comparison: $p>0.05$). There was no difference in the total degree of phasic depression between mitral cells and external tufted cells at any stimulus frequency tested (Figure 4 G), consistent with similar presynaptic properties of the incoming afferents.

However in mitral cells, phasic EPSCs were superimposed on a large, slow envelope current at all stimulus frequencies, reflecting the much larger dendrodendritic currents in mitral cells compared to external tufted cells (Figure 4 C; Vaaga & Westbrook, 2016). The total charge transfer was nearly 3 times larger in mitral cells (10 Hz: mitral cell: 219.9±50.6 pC, n=6 cells, external tufted cell: 84.4±23.25 pC, n=6 cells, Holm-Sidak post-hoc comparison: $p<0.05$; 25 Hz:

mitral cell: 268.0±43.4 pC, n=5 cells, external tufted cell: 75.5±24.7 pC, n=7 cells, Holm-Sidak post-hoc comparison: $p<0.01$; 50 Hz: mitral cell: 309.9±50.1 pC, n=7 cells, external tufted cell: 78.3±12.3 pC, n=7 cells; Holm-Sidak post-hoc comparison: $p<0.001$, Figure 4 F). Interestingly, the charge transfer was not sensitive to stimulation frequency (mitral cell: One way ANOVA: $p=0.43$; external tufted cell: One-way ANOVA: $p=0.96$, Figure 4 F), consistent with an all-or-none dendrodendritic slow EPSC (Carlson *et al.*, 2000; De Saint Jan *et al.*, 2009; Gire & Schoppa, 2009). Unlike the phasic responses, the degree of depression of the slow envelope current within the stimulus train was significantly different between mitral cells and external tufted cells (10 Hz: mitral cell: 57.1±3.2% of $EPSC_1$, external tufted cell 34.0±8.4% of $EPSC_1$, Holm-Sidak post-hoc comparison: $p<0.05$; 25 Hz: mitral cell: 67.2±10.2% of $EPSC_1$, external tufted cell: 33.9±5.5% of $EPSC_1$, Holm-Sidak post-hoc comparison: $p<0.01$; 50 Hz: mitral cell: 79.5±4.8% of $EPSC_1$, external tufted cell: 26.8±4% of $EPSC_1$, Holm-Sidak post-hoc comparison: $p<0.0001$; Figure 4 H).

In both mitral cells and external tufted cells, the depression of the phasic component was significantly larger than the depression of the slow, envelope current, and therefore all the data points fell above the unity line in a plot of phasic EPSC depression as a function of slow EPSC depression (Figure 4 I). Furthermore, the similarity of phasic depression and distinct slow current depression across cell types produced two identifiable clusters when the phasic and slow current depression are directly compared (Figure 4 I). Together this data suggests that a robust slow current supports sustained transmission in mitral cells, which is relatively insensitive to short-term depression and stimulus frequency.

The mitral cell slow current is responsible for sustained transmission

To explicitly test the role of the slow current in generating the sustained transmission in mitral cells, we blocked NMDA and mGluR1 receptors (10 μM CPP and 20 μM CPCCOEt, respectively), which effectively blocks the slow current in mitral cells (De Saint Jan & Westbrook, 2007; Vaaga & Westbrook, 2016). As expected, bath application of NMDA and mGluR1 antagonists reduced the total charge transfer in mitral cells (mitral cell: 309.9±50.1 pC, n=7 cells; mitral cell + CPP/CPCCOEt: 42.3±8.5 pC, n=6 cells, Holm-Sidak post-hoc comparison: $p<0.0001$, Figure 5 A, B), to levels comparable to the charge transfer in external tufted cells (external tufted cell: 78.27±12.26, n=7 cells, Holm-Sidak post-hoc comparison: $p>0.05$, Figure 5 B). Thus blocking the slow current converts the mitral cell response pattern to an external tufted cell pattern.

In cell attached recordings of mitral cells, blocking NMDA and mGluR1 receptors also caused a 4-fold reduction in the total number of spikes produced following 50 Hz stimulation (mitral cell: 161.8±27.2 spikes, n=7 cells; mitral cell + CPP/CPCCOEt: 37.62±7.3 spikes, n=5 cells, Holm-Sidak post-hoc comparison: $p<0.001$; external tufted cell: 45.2±9.0 spikes, n=8 cells; Holm-Sidak post-hoc comparison: $p>0.05$, Figure 5 D). Furthermore, bath application of NMDA and mGluR1 receptor antagonists also altered the temporal patterning of spikes, converting the sustained responses of mitral cells to more transient responses (extra sum of squares F-test: $p<0.001$, Figure 5 E), which were not significantly different than the responses in external tufted cells (extra sum of squares F-test: $p>0.05$, Figure 5 F). Together this data suggests that differences in the amplitude of the slow current between mitral cells and external tufted cells are responsible for the sustained transmission in mitral cells, and produce their distinct temporal spiking patterns.

Discussion:

In the glomerular microcircuit, the interplay of axodendritic and dendrodendritic synapses is critical to postsynaptic processing of afferent input. Although the glomerulus has long been viewed as a cortical module whose primary function is to enhance the signal-to-noise ratio (Chen & Shepherd, 2005), the synaptic dynamics in response to high frequency, naturalistic ORN stimulation have not previously been examined. Here we demonstrate that mitral cells and external tufted cells respond to high frequency afferent input with distinct temporal filters. Mitral cells produce sustained responses, requiring dendrodendritic amplification, whereas the lack of dendrodendritic amplification in external tufted cells results in transient responses. Together, our results indicate that the axodendritic and dendrodendritic circuits are functionally separable, and the relative balance of the two circuits determines the temporal filter of the postsynaptic cell.

Comparison with other synapses

Previous estimates of release probability using steady state measurements have suggested that the release probability of the ORN is near 1 (Murphy *et al.*, 2004). Our results using high frequency trains of stimuli suggest that the release probability of the ORN can be as high as 0.9 when presynaptic D_2 and $GABA_B$ receptors are blocked, however, in our experiments tonic and/or afferent evoked activation of presynaptic D_2 and $GABA_B$ receptors during high frequency trains reduces the release probability by approximately 30% in brain slices. Nonetheless, the presynaptic properties of olfactory receptor neurons are unusual, as compared with other synapses in the brain. Although many synapses, such as the climbing fiber synapse in the cerebellum, have a high release probability (Silver *et al.*, 1998; Dittman *et al.*, 2000), such

terminals generally show multi-vesicular release (Wadiche & Jahr, 2001; Rudolph *et al.,* 2015). However, the similar paired pulse ratio in control and low affinity antagonists suggest that ORN synapses operate using univesicular release (Murphy *et al.*, 2004; Taschenberger *et al.*, 2016). Another uniquantal, high release probability synapse exists in barrel cortex between layer 4 and layer 2/3 neurons (Silver *et al.*, 2003). However, in this case, the presynaptic neuron generally fires only 1-2 action potentials in response to whisker stimulation *in vivo* (Brecht & Sakmann, 2002), so synaptic depression resulting from high release probability does not impact the postsynaptic response. The univesicular, high release probability of the ORN, therefore, is unusual because individual ORNs fires at high frequencies in response to odorants (Sicard, 1986; Duchamp-Viret *et al.*, 1999; Carey *et al.*, 2009; Tan *et al.*, 2010).

In theory, the high frequency transmission of the ORN could be maintained despite a high initial release probability through multiple mechanisms including fast vesicle recycling (Kushmerick *et al.*, 2006; Saviane & Silver, 2006) and a second pool of low release probability vesicles (Lu & Trussell, 2016; Taschenberger *et al.*, 2016; Turecek *et al.*, 2016). These properties, however, appear to be absent in ORNs. In fact, the recovery of the fast EPSC following depletion was approximately 10 fold slower than at the calyx of Held (Kushmerick *et al.*, 2006), suggesting that individual ORNs may only transiently contribute to the postsynaptic response, thereby providing a rationale for the massive convergence of unimodal ORNs onto single glomeruli.

Axodendritic input is tuned to ensure faithful transmission

A striking feature of the glomerular microcircuit is the massive convergence of axons to a single glomerulus, with each axon carrying functionally redundant information (Mombaerts *et*

372 *al.*, 1996). This unimodal input is critical for odorant identification, as each odorant mixture
373 elicits a unique map of activated glomeruli, a so-called odor image (Xu *et al.*, 2000). However,
374 from a computational perspective, the massive redundancy is a waste of information channels
375 (Rieke, 1999; Chen & Shepherd, 2005). Furthermore, each olfactory receptor neuron responds to
376 increases in odorant concentration with monotonic increases in firing frequency, reaching up to
377 100 Hz (Sicard, 1986; Duchamp-Viret *et al.*, 1999; Carey *et al.*, 2009; Tan *et al.*, 2010). Coupled
378 with the high ORN release probability (Murphy *et al.*, 2004), trains of ORN activity produce
379 strong synaptic depression as demonstrated in our experiments, imposing a transient temporal
380 filter in postsynaptic cells, resulting from presynaptic vesicle depletion.

381 An advantage of such a high initial release probability is that odorant binding events in
382 the periphery are faithfully transmitted to the olfactory bulb in a nearly all-or-none manner. The
383 olfactory system is exquisitely sensitive, capable of detecting odorants at concentrations as low
384 as 1 part per 10^{15} molecules (Julius & Katz, 2004). In the periphery, this high sensitivity is
385 achieved through biochemical amplification downstream of G-protein coupled odorant receptors,
386 such that a single odorant receptor-binding event can elicit an action potential in the ORN
387 (Lynch & Barry, 1989). The high release probability of ORNs maintains the high sensitivity of
388 the olfactory system, by ensuring that ORN activity is faithfully converted to a postsynaptic
389 response. However, this circuit design comes at a cost in that individual nerve terminals can only
390 transiently contribute to postsynaptic activation, therefore requiring an ensemble of functionally
391 redundant channels to accurately convey information with high fidelity.

392

393 *Dendrodendritic circuitry promotes sustained transmission*

394 The high release probability of axodendritic input comes at another cost: the "noisy"
395 olfactory environment dramatically increases the total number of activated glomeruli in response
396 to ambient air. The signal to noise ratio, therefore, is enhanced through multiple mechanisms,
397 including the dendrodendritic amplification within the glomerulus (Carlson *et al.*, 2000; Chen &
398 Shepherd, 2005; De Saint Jan & Westbrook, 2007; Vaaga & Westbrook, 2016). The robust
399 increase in synaptic charge associated with the slow, dendrodendritic current effectively converts
400 the transient axodendritic input into a sustained spiking response, greatly amplifying afferent
401 input. Interestingly, our results indicate that only a subset of excitatory neurons, the mitral cells,
402 within the glomerulus express dendrodendritic amplification (Vaaga & Westbrook, 2016).
403
404 *Parallel input paths convey temporally distinct information*
405 Different principal neuron subtypes in the olfactory bulb represent parallel input
406 pathways. For example, *in vivo*, tufted cells respond to lower odorant concentrations, have
407 concentration invariant responses, and respond to odorants earlier in the sniff cycle (Nagayama
408 *et al.*, 2004; Igarashi *et al.*, 2012; Fukunaga *et al.*, 2012; Kikuta *et al.*, 2013). Mitral cells, on the
409 other hand, are more narrowly tuned than tufted cells, and shift their responses relative to the
410 sniff cycle in response to increasing odorant concentrations (Nagayama *et al.*, 2004; Kikuta *et*
411 *al.*, 2013). These *in vivo* results are consistent with the view that tufted cell responses maintain
412 the sensitivity of the ORN, via strong afferent evoked responses, whereas mitral cells provide
413 robust amplification, via strong dendrodendritic circuitry.
414 Recent evidence suggests that within piriform cortex the concentration invariant network
415 of activated pyramidal cells encodes odorant identity whereas concentration is encoded by the
416 temporal response profiles of pyramidal cells (Bolding & Franks, 2017). More specifically, the

417 spiking patterns of these pyramidal cells have two distinct peaks, one with a short latency and
418 one with a longer latency. As concentration increases, the relative lag between these two
419 responses is shortened (Bolding & Franks, 2017). Mechanistically, this may result from the
420 integration of olfactory bulb projection neurons that express strong axodendritic input,
421 contributing to the short latency, concentration invariant response, and neurons that express
422 strong dendrodendritic input, with variable, concentration-dependent delays. Such an activation
423 scheme, however, would require overlapping projection patterns in piriform cortex. Single axon
424 tracing studies, however, suggest that mitral cells and tufted cells project to largely non-
425 overlapping regions of olfactory cortex (Igarahsi *et al*., 2012). More specifically, mitral cells
426 project to dorsal region of the anterior piriform cortex as well as the cortical region of the
427 olfactory tubercle, posterior piriform cortex and tenia tecta; whereas tufted cells, including
428 external tufted cells, project to the ventrorostral anterior piriform cortex, the cap of the olfactory
429 tubercle, and the pars extrema and the poteroventral region of the anterior olfactory nucleus.
430 (Igarashi *et al.*, 2012). Resolving the exact projection patterns and mechanisms behind
431 generating distinct timing signals in piriform cortex is critical to understanding the encoding of
432 concentration within the olfactory system. Our results, however, demonstrate that the distinct
433 balance of axodendritic and dendrodendritic synaptic strength in each principal cell population
434 likely contributes to the unique computations within these parallel input pathways, by imposing
435 unique temporal filters in each cell type.
436
437

438 **References:**

439 Abbott LF & Regehr WG (2004). Synaptic computation. *Nature* **431,** 796–803.
440 Aroniadou-Anderjaska V, Zhou F-M, Priest CA, Ennis M & Shipley MT (2000). Tonic and

441 Synaptically Evoked Presynaptic Inhibition of Sensory Input to the Rat Olfactory Bulb Via
442 GABABHeteroreceptors. *J Neurophysiol* **84,** 1194–1203.

443 Betz WJ (1970). Depression of transmitter release at the neuromuscular junction of the frog. *J*
444 *Physiol* **206,** 629–644.

445 Bolding KA & Franks KM (2017). Complementary codes for odor identity and intensity in
446 olfactory cortex. *Elife*; DOI: 10.7554/eLife.22630.

447 Brecht M & Sakmann B (2002). Dynamic representation of whisker deflection by synaptic
448 potentials in spiny stellate and pyramidal cells in the barrels and septa of layer 4 rat
449 somatosensory cortex. *J Physiol* **543,** 49–70.

450 Carey RM, Verhagen JV, Wesson DW, Pírez N & Wachowiak M (2009). Temporal structure of
451 receptor neuron input to the olfactory bulb imaged in behaving rats. *J Neurophysiol* **101,**
452 1073–1088.

453 Carlson GC, Shipley MT & Keller A (2000). Long-lasting depolarizations in mitral cells of the
454 rat olfactory bulb. *J Neurosci* **20,** 2011–2021.

455 Chanda S & Xu-Friedman MA (2010). A low-affinity antagonist reveals saturation and
456 desensitization in mature synapses in the auditory brain stem. *J Neurophysiol* **103,** 1915–
457 1926.

458 Chen WR & Shepherd GM (2005). The olfactory glomerulus: a cortical module with specific
459 functions. *J Neurocytol* **34,** 353–360.

460 De Saint Jan D, Hirnet D, Westbrook GL & Charpak S (2009). External tufted cells drive the
461 output of olfactory bulb glomeruli. *J Neurosci* **29,** 2043–2052.

462 De Saint Jan D & Westbrook GL (2007). Disynaptic amplification of metabotropic glutamate
463 receptor 1 responses in the olfactory bulb. *J Neurosci* **27,** 132–140.

464 Dittman JS, Kreitzer AC & Regehr WG (2000). Interplay between facilitation, depression, and
465 residual calcium at three presynaptic terminals. *J Neurosci* **20,** 1374–1385.

466 Duchamp-Viret P, Chaput MA & Duchamp A (1999). Odor response properties of rat olfactory
467 receptor neurons. *Science* **284,** 2171–2174.

468 Elmqvist D & Quastel DM (1965). A quantitative study of end-plate potentials in isolated human
469 muscle. *J Physiol* **178,** 505–529.

470 Ennis M, Zhou F-M, Ciombor KJ, Aroniadou-Anderjaska V, Hayar A, Borrelli E, Zimmer LA,
471 Margolis F & Shipley MT (2001). Dopamine D2 Receptor–Mediated Presynaptic Inhibition
472 of Olfactory Nerve Terminals. *J Neurophysiol* **86,** 2986–2997.

473 Foster KA, Kreitzer AC & Regehr WG (2002). Interaction of postsynaptic receptor saturation
474 with presynaptic mechanisms produces a reliable synapse. *Neuron* **36,** 1115–1126.

475 Fukunaga I, Berning M, Kollo M, Schmaltz A & Schaefer AT (2012). Two distinct channels of
476 olfactory bulb output. *Neuron* **75,** 320–329.

477 Geramita M & Urban NN (2017). Differences in Glomerular-Layer-Mediated Feedforward
478 Inhibition onto Mitral and Tufted Cells Lead to Distinct Modes of Intensity Coding. *J*
479 *Neurosci* **37,** 1428–1438.

480 von Gersdorff H & Borst JGG (2002). Short-term plasticity at the calyx of Held. *Nat Rev*
481 *Neurosci* **3,** 53–64.

482 Giraudet P, Berthommier F & Chaput M (2002). Mitral cell temporal response patterns evoked
483 by odor mixtures in the rat olfactory bulb. *J Neurophysiol* **88,** 829–838.

484 Gire DH, Franks KM, Zak JD, Tanaka KF, Whitesell JD, Mulligan AA, Hen R & Schoppa NE
485 (2012). Mitral cells in the olfactory bulb are mainly excited through a multistep signaling
486 path. *J Neurosci* **32,** 2964–2975.

487 Gire DH & Schoppa NE (2009). Control of on/off glomerular signaling by a local GABAergic
488 microcircuit in the olfactory bulb. *J Neurosci* **29,** 13454–13464.

489 Hayar A, Shipley MT & Ennis M (2005). Olfactory bulb external tufted cells are synchronized
490 by multiple intraglomerular mechanisms. *J Neurosci* **25,** 8197–8208.

491 Igarashi KM, Ieki N, An M, Yamaguchi Y, Nagayama S, Kobayakawa K, Kobayakawa R,
492 Tanifuji M, Sakano H, Chen WR & Mori K (2012). Parallel mitral and tufted cell pathways
493 route distinct odor information to different targets in the olfactory cortex. *J Neurosci* **32,**
494 7970–7985.

495 Jahr CE & Nicoll RA (1980). Dendrodendritic inhibition: demonstration with intracellular
496 recording. *Science* **207,** 1473–1475.

497 Jahr CE & Nicoll RA (1982). An intracellular analysis of dendrodendritic inhibition in the turtle
498 in vitro olfactory bulb. *J Physiol* **326,** 213–234.

499 Julius D & Katz LC (2004). A Nobel for smell. *Cell* **119,** 747–752.

500 Kikuta S, Fletcher ML, Homma R, Yamasoba T & Nagayama S (2013). Odorant response
501 properties of individual neurons in an olfactory glomerular module. *Neuron* **77,** 1122–1135.

502 Kiyokage E, Pan Y-Z, Shao Z, Kobayashi K, Szabo G, Yanagawa Y, Obata K, Okano H, Toida
503 K, Puche AC & Shipley MT (2010). Molecular identity of periglomerular and short axon
504 cells. *J Neurosci* **30,** 1185–1196.

505 Kushmerick C, Renden R & von Gersdorff H (2006). Physiological temperatures reduce the rate
506 of vesicle pool depletion and short-term depression via an acceleration of vesicle
507 recruitment. *J Neurosci* **26,** 1366–1377.

508 Leng G, Hashimoto H, Tsuji C, Sabatier N & Ludwig M (2014). Discharge patterning in rat

olfactory bulb mitral cells in vivo. *Physiol Rep*; DOI: 10.14814/phy2.12021.

Liley AW & North KA (1953). An electrical investigation of effects of repetitive stimulation on mammalian neuromuscular junction. *J Neurophysiol* **16,** 509–527.

Lu H-W & Trussell LO (2016). Spontaneous Activity Defines Effective Convergence Ratios in an Inhibitory Circuit. *J Neurosci* **36,** 3268–3280.

Lynch JW & Barry PH (1989). Action potentials initiated by single channels opening in a small neuron (rat olfactory receptor). *Biophys J* **55,** 755–768.

Maher BJ & Westbrook GL (2008). Co-transmission of dopamine and GABA in periglomerular cells. *J Neurophysiol* **99,** 1559–1564.

Mennerick S & Matthews G (1996). Ultrafast exocytosis elicited by calcium current in synaptic terminals of retinal bipolar neurons. *Neuron* **17,** 1241–1249.

Mombaerts P, Wang F, Dulac C, Chao SK, Nemes A, Mendelsohn M, Edmondson J & Axel R (1996). Visualizing an olfactory sensory map. *Cell* **87,** 675–686.

Murphy GJ, Glickfeld LL, Balsen Z & Isaacson JS (2004). Sensory neuron signaling to the brain: properties of transmitter release from olfactory nerve terminals. *J Neurosci* **24,** 3023–3030.

Nagayama S, Takahashi YK, Yoshihara Y & Mori K (2004). Mitral and tufted cells differ in the decoding manner of odor maps in the rat olfactory bulb. *J Neurophysiol* **91,** 2532–2540.

Najac M, De Saint Jan D, Reguero L, Grandes P & Charpak S (2011). Monosynaptic and polysynaptic feed-forward inputs to mitral cells from olfactory sensory neurons. *J Neurosci* **31,** 8722–8729.

Neher E (2015). Merits and Limitations of Vesicle Pool Models in View of Heterogeneous Populations of Synaptic Vesicles. *Neuron* **87,** 1131–1142.

Nickell WT, Behbehani MM & Shipley MT (1994). Evidence for GABAB-mediated inhibition of transmission from the olfactory nerve to mitral cells in the rat olfactory bulb. *Brain Res Bull* **35,** 119–123.

Regehr WG (2012). Short-term presynaptic plasticity. *Cold Spring Harb Perspect Biol* **4,** a005702.

Rieke F (1999). *Spikes: exploring the neural code*. MIT press.

Rospars J-P, Lánský P, Duchamp A & Duchamp-Viret P (2003). Relation between stimulus and response in frog olfactory receptor neurons in vivo. *Eur J Neurosci* **18,** 1135–1154.

Rudolph S, Tsai MC, von Gersdorff H, Wadiche, JI (2015). The ubiquitous nature of multivesicular release. *Trends Neurosci* **38**,428-438.

Sakaba T & Neher E (2001). Calmodulin mediates rapid recruitment of fast-releasing synaptic

vesicles at a calyx-type synapse. *Neuron* **32,** 1119–1131.

Saviane C & Silver RA (2006). Fast vesicle reloading and a large pool sustain high bandwidth transmission at a central synapse. *Nature* **439,** 983–987.

Schneggenburger R, Meyer AC & Neher E (1999). Released fraction and total size of a pool of immediately available transmitter quanta at a calyx synapse. *Neuron* **23,** 399–409.

Schneggenburger R, Sakaba T & Neher E (2002). Vesicle pools and short-term synaptic depression: lessons from a large synapse. *Trends Neurosci* **25,** 206–212.

Schoppa NE & Westbrook GL (2001). Glomerulus-specific synchronization of mitral cells in the olfactory bulb. *Neuron* **31,** 639–651.

Shao Z, Puche AC, Kiyokage E, Szabo G & Shipley MT (2009). Two GABAergic intraglomerular circuits differentially regulate tonic and phasic presynaptic inhibition of olfactory nerve terminals. *J Neurophysiol* **101,** 1988–2001.

Shao Z, Puche AC, Liu S & Shipley MT (2012). Intraglomerular inhibition shapes the strength and temporal structure of glomerular output. *J Neurophysiol* **108,** 782–793.

Shao Z, Puche AC & Shipley MT (2013). Intraglomerular inhibition maintains mitral cell response contrast across input frequencies. *J Neurophysiol* **110,** 2185–2191.

Sicard G (1986). Electrophysiological recordings from olfactory receptor cells in adult mice. *Brain Res* **397,** 405–408.

Silver RA, Lubke J, Sakmann B & Feldmeyer D (2003). High-probability uniquantal transmission at excitatory synapses in barrel cortex. *Science* **302,** 1981–1984.

Silver RA, Momiyama A & Cull-Candy SG (1998). Locus of frequency-dependent depression identified with multiple-probability fluctuation analysis at rat climbing fibre-Purkinje cell synapses. *J Physiol* **510 (Pt 3),** 881–902.

Tan J, Savigner A, Ma M & Luo M (2010). Odor information processing by the olfactory bulb analyzed in gene-targeted mice. *Neuron* **65,** 912–926.

Taschenberger H, Woehler A & Neher E (2016). Superpriming of synaptic vesicles as a common basis for intersynapse variability and modulation of synaptic strength. *Proc Natl Acad Sci U S A* **113,** E4548–E4557.

Taschenberger H, Leão RM, Rowland KC, Spirou GA & von Gersdorff H (2002). Optimizing synaptic architecture and efficiency for high-frequency transmission. *Neuron* **36,** 1127–1143.

Thanawala MS & Regehr WG (2016). Determining synaptic parameters using high-frequency activation. *J Neurosci Methods* **264,** 136–152.

576 Trussell LO, Zhang S & Raman IM (1993). Desensitization of AMPA receptors upon
577 multiquantal neurotransmitter release. *Neuron* **10,** 1185–1196.

578 Turecek J, Jackman SL & Regehr WG (2016). Synaptic Specializations Support Frequency-
579 Independent Purkinje Cell Output from the Cerebellar Cortex. *Cell Rep* **17,** 3256–3268.

580 Vaaga CE & Westbrook GL (2016). Parallel processing of afferent olfactory sensory
581 information. *J Physiol* **594,** 6715–6732.

582 Vaaga CE, Yorgason JT, Williams JT & Westbrook GL (2017). Presynaptic gain control by
583 endogenous cotransmission of dopamine and GABA in the olfactory bulb. *J Neurophysiol*
584 **117,** 1163–1170.

585 Wachowiak M, McGann JP, Heyward PM, Shao Z, Puche AC & Shipley MT (2005). Inhibition
586 of Olfactory Receptor Neuron Input to Olfactory Bulb Glomeruli Mediated by Suppression
587 of Presynaptic Calcium Influx. *J Neurophysiol* **94,** 2700–2712.

588 Wadiche JI & Jahr CE (2001). Multivesicular release at climbing fiber-Purkinje cell synapses.
589 *Neuron* **32,** 301–313.

590 Wang LY & Kaczmarek LK (1998). High-frequency firing helps replenish the readily releasable
591 pool of synaptic vesicles. *Nature* **394,** 384–388.

592 Wong AYC, Graham BP, Billups B & Forsythe ID (2003). Distinguishing between presynaptic
593 and postsynaptic mechanisms of short-term depression during action potential trains. *J*
594 *Neurosci* **23,** 4868–4877.

595 Xu F, Greer CA & Shepherd GM (2000). Odor maps in the olfactory bulb. *J Comp Neurol* **422,**
596 489–495.

597

598

599 **Figure Legends:**

600

601 Figure 1: **Sustained transmission in mitral and external tufted cells** (**A**) Cell attached
602 recording from mitral cell in response to 50 Hz ORN stimulation. (**B**) Raster plot of mitral cell
603 response. Mitral cells responded to ORN stimulation with sustained responses, which outlasted
604 the stimulus. (**C**) Cell attached recording and (**D**) associated raster plot of external tufted cell
605 response to 50 Hz ORN stimulation. External tufted cells produced much more transient
606 response profiles. (**E**) Plot of the average number of action potentials produced following each
607 stimulus in the train. Mitral cells and external tufted cells produce similar numbers of action
608 potentials at the beginning of the train. By the end of the train, however, mitral cells produce
609 approximately twice as many action potentials as external tufted cells. (**F**) The total number of
610 spikes produced (within 2.5 seconds) in mitral cells is significantly higher than in external tufted
611 cells. (**G**) Plot of the fraction of total spikes in the train as a function of stimulus number. Mitral
612 cells (black) have a more shallow relationship, consistent with sustained transmission. External
613 tufted cells (red) have a significantly steeper relationship, indicative of transient response
614 profiles.

615

616 Figure 2: **Olfactory receptor neurons have a high release probability** (**A_1, B_1**) Representative
617 whole-cell voltage clamp responses to 50 Hz stimulation in mitral cells (**A_1**, black) and external
618 tufted cells (**B_1**, red). (**A_2, B_2**) Estimates of the readily releasable pool size using the SMN train
619 method in mitral cells (**A_2**) and external tufted cells (**B_2**). (**A_3, B_3**) Estimate of readily releasable
620 pool size using the EQ method in mitral cells (**A_3**) and external tufted cells (**B_3**). (**C**) Estimates
621 of release probability do not differ between the Schneggenburger (SMN) and Elmqvist-Quastal

(EQ) methods. There was also no significant difference between the release probability calculated in mitral cells (black) and external tufted cells (red). (**D**) Paired pulse ratio in external tufted cells before (black) and after (green) addition of 2 mM kynurenic acid to prevent receptor saturation and desensitization. Response in kynurenic acid scaled to control (red). (**E**) Summary of the paired pulse ratio in external tufted cells before and after 2 mM kynurenic acid, suggesting postsynaptic saturation and desensitization do not contribute to synaptic depression.

Figure 3: **Single pool of slowly recycling vesicles** (**A**) Representative external tufted cell recording showing 10 Hz stimulation followed by 50 Hz stimulation. (**B**) Group data shows immediate depression following 10 Hz stimulation, suggesting a single pool of synaptic vesicles. (**C**) Plot of the phasic EPSC amplitude as a function of stimulus number is fit by a single exponential, further suggesting a single pool of high release probability vesicles. (**D, E**) Recovery of phasic EPSC amplitude following 50 Hz stimulation suggests that vesicle replenishment is slow. (**F**) Recovery time course is best fit by a double exponential.

Figure 4: **Differential modulation of phasic and slow currents in mitral and external tufted cells** (**A, B**) Whole-cell voltage clamp responses of mitral cells (**A**, black) and external tufted cells (**B**, red) to stimulation at various frequencies (10, 25, 50 Hz). (**C**) Comparison of the slow, envelope current measured in mitral cells (grey) and external tufted cells (pink) at each stimulus frequency. Mitral cells had consistently larger envelope currents. (**D**) Depression of the phasic EPSC amplitude as a function of stimulus number in mitral cells across stimulation frequencies (blue: 10 Hz, red: 25 Hz, black: 50 Hz). (**E**) Depression of phasic EPSC amplitude as a function of stimulus number in external tufted cells (colors as in **D**). (**F**) The total charge transfer

(measured 2.5 seconds after stimulus onset) was significantly larger in mitral cells than external tufted cells across all stimulation frequencies. There was no significant difference across stimulus frequencies within either cell type. (**G**) Total phasic depression in mitral cells (black) and external tufted cells (red) across stimulation frequencies. There was no significant difference between cell types at any frequency tested. (**H**) Total slow current depression in mitral cells (black) and external tufted cells (red) across stimulation frequencies. Mitral cells had significantly less slow current depression at all stimulus frequencies tested. (**I**) Plot showing a direct comparison of phasic depression and tonic depression across cell types and frequencies (blue: 10 Hz, red: 25 Hz, black: 50 Hz). Although the phasic depression was similar between cell types and frequencies, the slow current was differentially regulated in mitral cells and external tufted cells.

Figure 5: **Blocking the slow current converts mitral cell responses into external tufted cell responses** (**A**) Peak scaled comparison of the whole cell voltage clamp recordings from mitral cells in control (black) and 10 μM CPP/20 μM CPCCOEt (green) in response to 50 Hz ORN stimulation. As expected, CPP/CPCCOEt blocked a significant portion of the slow envelope current. (**B**) Comparison of the total charge transfer in mitral cells (black), external tufted cells (red) and mitral cells with CPP/CPCCOEt (green) shows that blocking the NMDA/mGluR1 receptor dependent current significantly reduces the total charge transfer to levels comparable to external tufted cells. (**C**) Cell-attached recording from mitral cell in response to 50 Hz ORN stimulation shows transient spiking profile mitral cells when NMDA and mGluR1 receptors are blocked. (**D**) The total number of action potentials produced in mitral cells with NMDA and mGluR1 receptors are similar to external tufted cell responses. (**E**) Comparison of the temporal

668 profile of mitral cell spiking in control (black) and with CPP/CPCCOEt (green). Block of
669 NMDA and mGluR1 receptors reveal transient response profile of mitral cells. (**F**) With NMDA
670 and mGluR1 receptors blocked, the temporal profile of mitral cell spiking (green) is not
671 significantly different than the responses of external tufted cells (red).
672

Figure 1

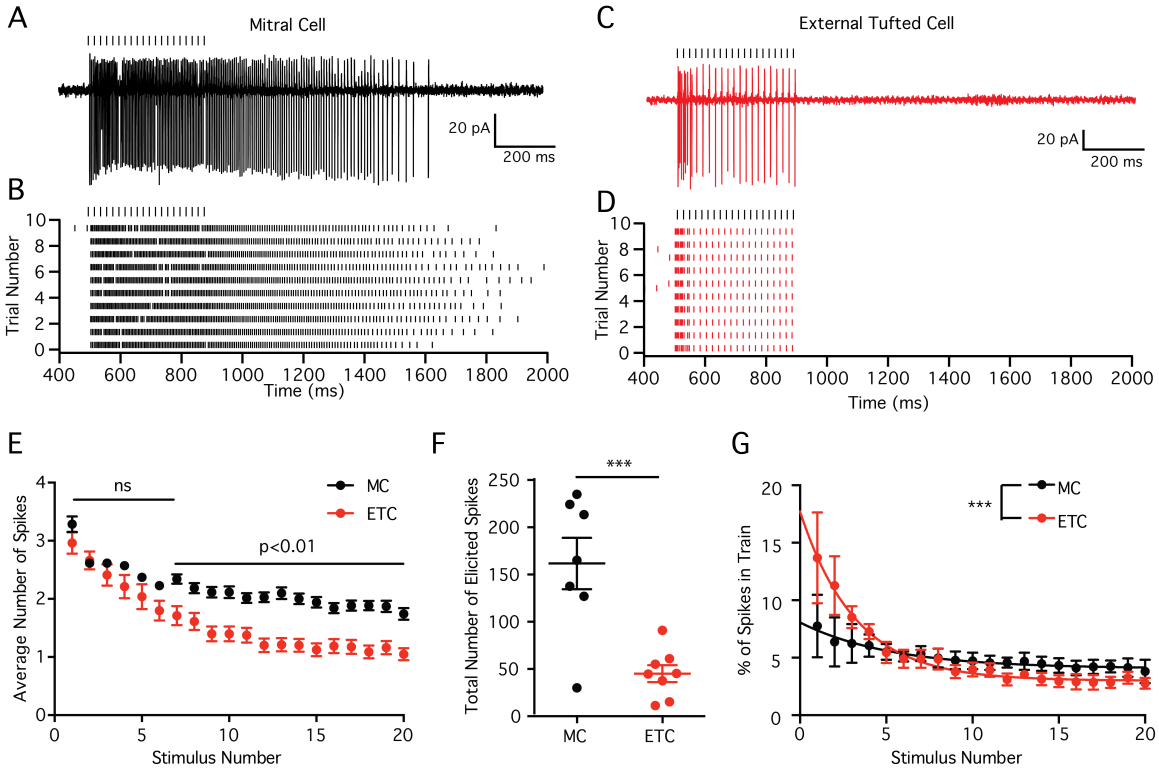

Figure 2

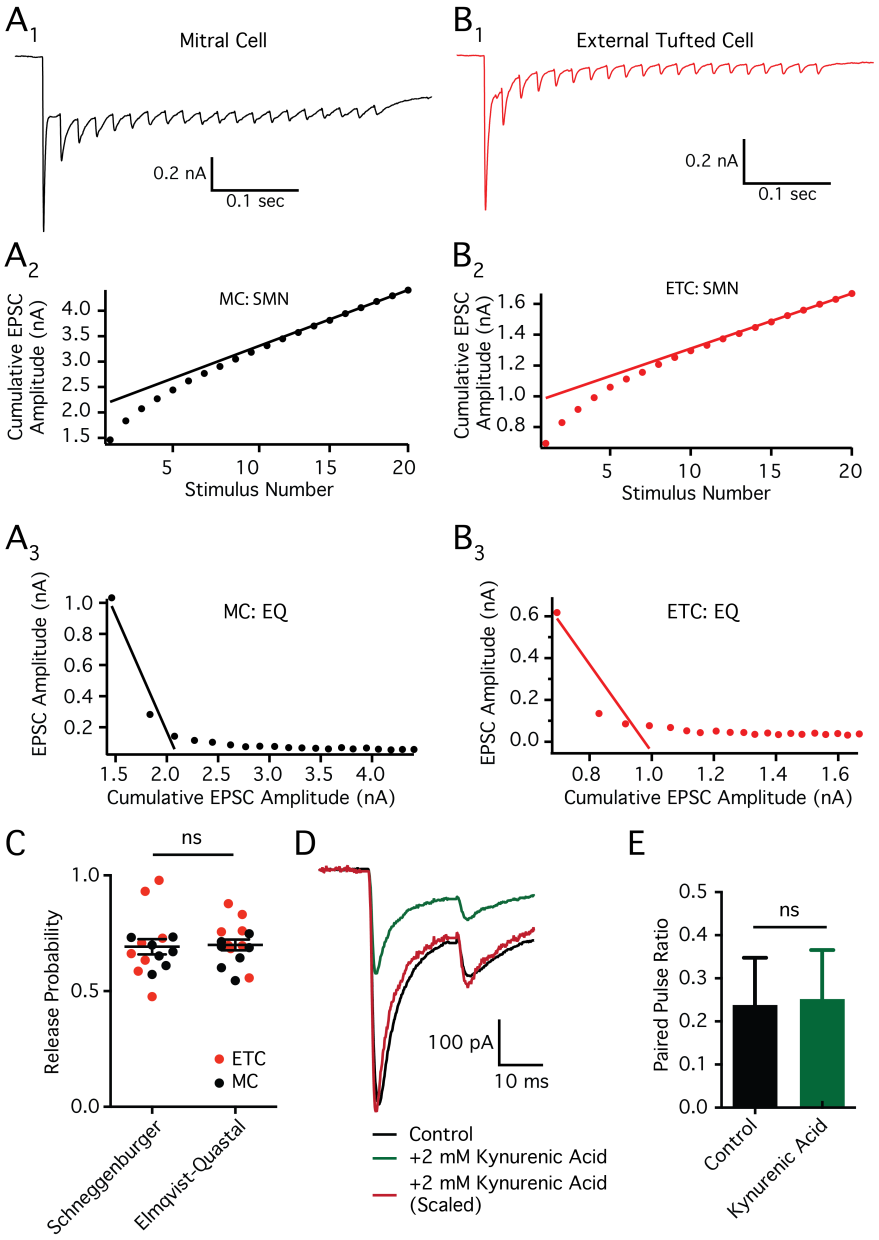

Figure 3

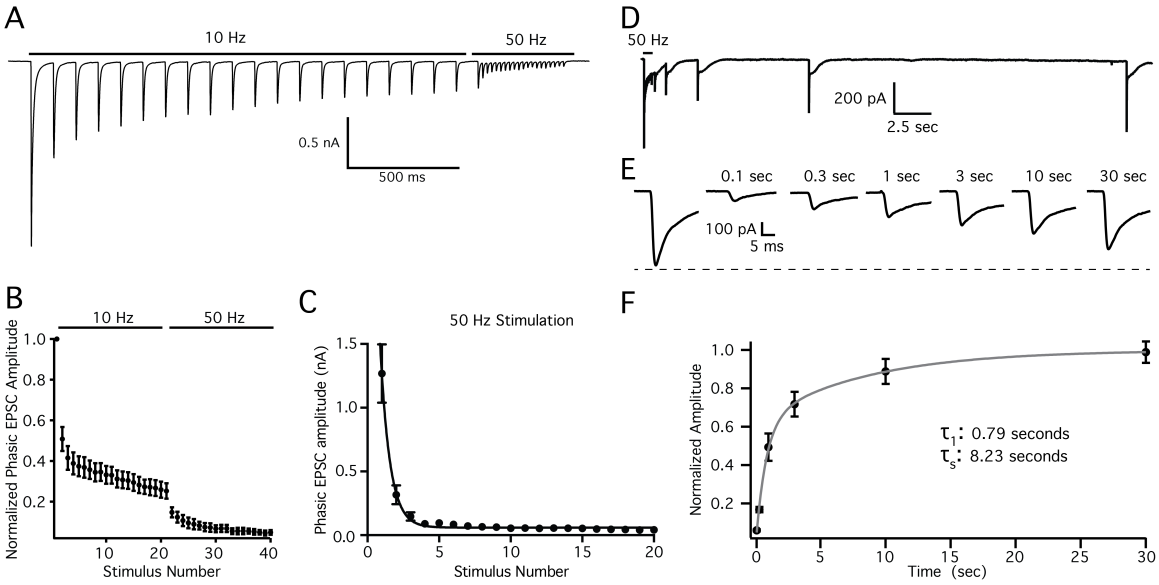

Figure 4

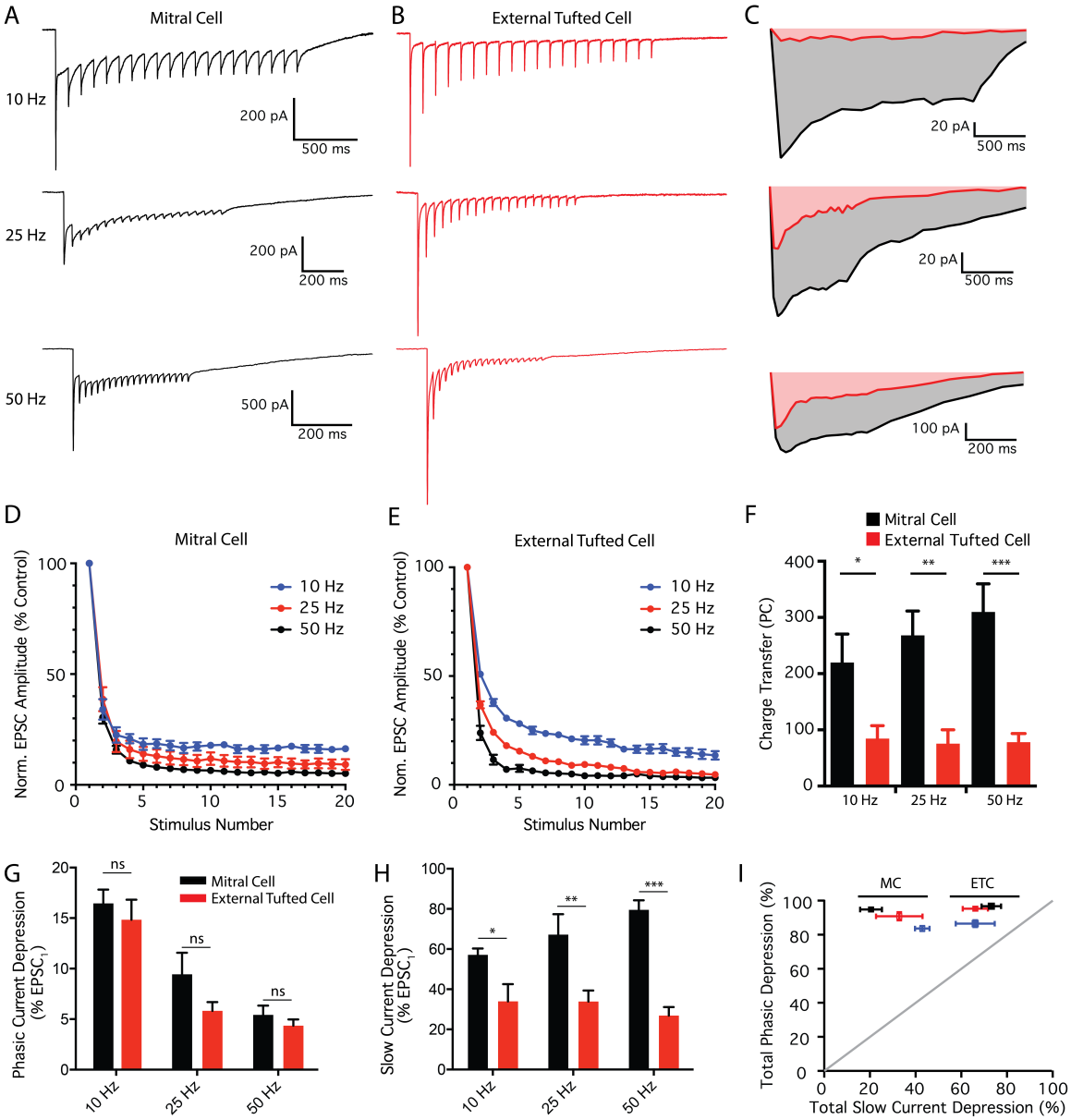

Figure 5